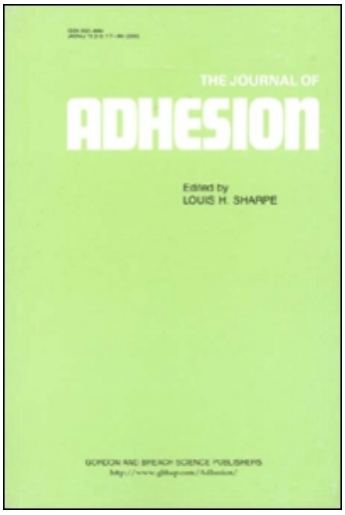

The Journal of Adhesion
Publication details, including instructions for authors and subscription information:
http://www.informaworld.com/smpp/title~content=t713453635

Mechanisms of Adhesive Bond Endurance: Steel-Epoxy under Hydrothermal Stress

Tennyson Smith[a]
[a] Rockwell International Science Center, Thousand Oaks, CA, U.S.A.

Online publication date: 02 December 2010

To cite this Article Smith, Tennyson(1984) 'Mechanisms of Adhesive Bond Endurance: Steel-Epoxy under Hydrothermal Stress', The Journal of Adhesion, 17: 1, 1 — 20
To link to this Article: DOI: 10.1080/00218468408078426
URL: http://dx.doi.org/10.1080/00218468408078426

J. Adhesion, 1984, Vol. 17, pp. 1–20
0021–8464/84/1701–0001 $18.50/0

Printed in the United Kingdom

Mechanisms of Adhesive Bond Endurance: Steel-Epoxy under Hydrothermal Stress

TENNYSON SMITH

Rockwell International Science Center, 1049 Camino dos Rios, Thousand Oaks, CA 91360, U.S.A.

Stainless steel (AM 355) has been given a number of surface treatments in preparation for adhesive bonding with modified 121 C curing epoxy. The treatments divide into two groups, those that result in very durable joints under hydrothermal stress and those that do not. Those treatments that provide endurance have a chromium-oxide rich outer layer; those that do not have an iron-oxide outer layer. Strongly oxidizing solutions (acids with dichomate) and anodic treatments cause selective dissolution of Fe and reprecipitation of a dentritic layer (~ 500Å) of an intermetallic compound of Cr, Ni and Mo. These dentrites (covered with a thin chromium oxide layer) form a capillary network that draws adhesive into the network, providing mechanical interlocking. However, the crucial criterion for endurance lies in the chemisorbed layer that results from the treatment. If reaction with water goes to completion in the oxidizing solution, the surface is covered with basic OH^- which can strongly bond with acid functional groups of the epoxy. Since the surface reaction has gone to completion with respect to water, there is no thermodynamic driving force for post-bond reactions in humid atmosphere. Those treatments that do not go to completion form strong bonds with the adhesive, but degrade under hydrothermal stress in post-bond conditions as the water reactions continue to completion.

INTRODUCTION

In a previous paper[1] a complete description is given of the effect of various surface treatments on the hydrothermal-stress endurance of AM 355 stainless steel bonded with 121°C (250°F) curing modified

Presented at the Annual Meeting of The Adhesion Society, Mobile, AL, U.S.A., February 21–24, 1982.

epoxy. In this paper mechanisms by which bond degradation occurs and the principles on which improved endurance can be attained are described.

EXPERIMENTAL

The experimental approach is designed to correlate endurance with surface properties that result from the various surface treatments.[1] The "Wedge Test" (ASTM-D3726-29) is the primary test for hydrothermal-stress endurance. After bonding, a wedge is forced into the bond to provide an initial crack which arrests when the stress at the crack tip is just equal to the fracture toughness. The wedged joint is then placed in a humidity chamber (60°C, 100% RH) and the crack extension monitored at 1 h and 24 h. Although the reaction rate at the crack tip is not constant with time,[2] as an approximation we use the crack extension at 24 h as the rate for comparative purposes.

Surface properties were monitored, prior to bonding, with seven surface techniques: scanning electron microscopy (SEM), Auger electron spectroscopy (AES), x-ray photoelectron spectroscopy (XPS), ellipsometry, contact potential difference (CPD), photoelectron emission (PEE), and water contact angle measurement. The methods and interpretation of results from the last three tools have been discussed in a previous paper.[3] The water contact angles were measured by the sessile drop technique, with a Ramé-Hart goniometer.

EXPERIMENTAL RESULTS

Durability from Chemistry

Table 1 lists the surface treatments in order of decreasing crack extension (increasing durability) under hydrothermal stress. The Auger peak-to-peak heights (APPH) for Fe, Cr, C and O in Table 1 are given for the outer atomic layers (first 20 Å) prior to Ar^+ sputtering. The ratio of the Cr peak to the Fe peak at the surface is labeled (outside) and the ratio of Cr/Fe, after a minute of sputtering, is labeled (inside) in Table 1. In the right hand columns of Table 1 are listed the values of CPD, PEE, film thickness d_1 (estimated from sputter-back etching), d_2 (from ellipsometry), film index of refraction, n, and film absorption index, κ

TABLE I
Surface properties and "wedge test" results as a function of surface treatment

Surface Treatment	No.	Chemical Surface Properties Auger (APPH) Fe outside	Cr outside	Cr/Fe outside[b]	Cr/Fe inside[c]	C outside	O outside	Physical Surface Properties CPD (V)	PEE (nano-amp)	d_1[a] Å	d_2 Å	n	κ	Endurance θH_2O (deg)	Δa (cm/24 h)
Degrease	1	0.4	0.0	0.0	0.3	1.1	2.5	+0.07	0.90	50	115	2.0	0.0	65	6.86
$KMnO_4$/NaOH	6b	0.5	0.0	0.0	0.3	0.6	4.2	−0.45	0.70	100	110	2.5	0.1	50	2.54
Flame	18f	0.5	0.0	0.0	0.0	0.5	4.8	−0.23	4.60	>650	364	2.5	0.1	38	2.29
MICRO-UV	19b	0.8	0.0	0.0	0.2	0.7	4.7	−0.09	1.40	70	90	1.4	0.0	66	1.52
HNO_3	9a	0.5	0.9	1.8	1.0	0.8	4.7	−0.21	1.20	30	20	1.5	0.0	40	0.89
H_2SO_4-CrO_3- anodize	5	0.5	0.7	1.4	1.3	0.3	5.2	−0.31	0.40	30	157	2.6	0.5	38	0.76
H_2SO_4-HNO_3-dichromate	13b	—	—	—	—	—	—	−0.82	0.38	—	240	2.5	0.0	0	0.40
H_2SO_4-HNO_3	13a	0.4	1.1	2.7	2.3	0.5	5.1	−0.24	1.70	80	111	2.4	0.3	7	0.25
HNO_3-dichromate	9f	0.4	1.0	2.5	3.0	0.9	6.3	−0.72	0.51	130	186	2.6	0.0	3	0.25
H_2SO_4- dichromate-anodize	7	0.3	0.8	2.7	2.4	0.3	6.5	−0.52	0.22	>200	216	2.6	0.6	0	0.15
H_2SO_4-dichromate	12e	0.5	1.6	3.2	4.1	0.5	9.6	−0.96	0.18	1050	578	2.7	0.4	0	0.15
HNO_3-anodize	10h	0.5	0.8	0.8	2.0	0.3	4.5	−0.32	1.00	80	117	2.6	0.6	7	0.13

[a] d_1 from sputter back etching, assume sputter rate of 21 Å/min, d_2 from ellipsometry.
[b] Outside refers to outside atomic layers.
[c] Inside refers to inside the oxide film.

(from ellipsometry), θH_2O, and Δa (crack extension in 24 h).

Table 1 is divided into two surface treatment groups, those that result in $\Delta a \geq 0.76$ cm/24 h and those for $\Delta a \leq 0.40$ cm/24 h. The dramatic distinguishing surface properties in these groups are: Cr/Fe ratio, oxygen APPH, and θH_2O. The Cr/Fe ratio is 2 to 3 times as large in the high endurance group, oxygen is higher, and θH_2O drops from a low of 38° in the low endurance group to $< 7°$ in the high endurance group. This difference in θH_2O does not correlate with carbonaceous contamination since, except for the degrease-only treatment, the APPH(C) is approximately constant, as is the APPH(Fe). However, the large θH_2O values could result from carbonaceous contamination if it is removed by evacuation in the UHV system. If the degrease-only treatment in MEK leaves about one monolayer of MEK, the other treatments leave about half a monolayer. This is true even for the high endurance group.

Concentrating on one of the best treatments (12e), Table 2 lists the surface properties and Δa as a function of wt % dichromate in the sulfuric acid solution at 80°C for 60 min. There are systematic trends in surface properties with increasing dichromate concentration. The film thickness increases from about 144 Å to 574Å. The refractive index is close to that for iron and chromium oxide (~ 2.6) but the absorption index is much larger for solutions with dichromate, indicating a film with strong light absorption. The CPD becomes increasingly negative, indicating increasing concentration of dipoles with negative end pointing away from the surface (*i.e.*, increasing chemisorbed oxygen). The PEE decreases, indicating attenuation of the electron emission from the substrate as the film thickens. Note that although the water contact

TABLE II
Effect of Dichromate on the Surface Properties and Bond Endurance of Stainless Steel. T = 80°C, t = 60 min.

wt % Dichromate	d (Å)	n	κ	CPD (V)	PEE (nanoamp)	θH_2O (deg)	Δa (cm/24 h)
0	144	2.6	0.08	+0.17	1.70	46	3.2
1	257	2.6	0.9	−0.17	0.29	16	4.3
2	304	2.6	0.8	−0.25	0.25	16	3.8
5	420	2.7	0.5	−0.22	0.16	12	3.8
10	433	2.7	0.4	−0.44	0.14	11	3.6
40	574	2.7	0.4	−0.96	0.18	0	0.18

TABLE III
Effect of time and temperature on surface properties and bond endurance for stainless steel in H_2SO_4/dichromate

Temp (°C)	Immersion Time	d (Å)	n	κ	CPD (V)	PEE (nanoamp)	Δa (cm/24 h)
23	60	90	1.8	0.0	−0.58	0.50	0.89
40	60	10	2.0	0.0	−0.66	0.51	0.36
50	60	16	2.0	0.0	−0.68	0.35	0.38
60	60	255	2.6	0.3	−0.74	0.64	0.36
70	60	633	2.6	0.4	−0.96	0.18	0.18
23	0	115	1.9	0.0	+0.07	0.90	6.40
	30	77	2.0	0.0	−0.62	0.62	3.00
	60	91	1.8	0.0	−0.58	0.50	0.89
	90	71	2.0	0.0	−0.68	0.50	1.40
	120	80	1.8	0.0	−0.65	0.50	0.51
80	0	115	1.9	0.0	+0.07	0.90	6.40
	30	632	2.7	0.4	−0.94	0.14	0.36
	60	574	2.7	0.4	−0.96	0.18	0.18
	90	382	3.3	0.3	−1.00	0.16	0.15
	120	500	2.9	0.4	−0.86	0.18	0.30

angles are low ($< 16°$), the crack extension Δa is high. This indicates that surface cleanliness may be necessary but is not sufficient to provide enduring bonds. The one outstanding feature associated with the low Δa of 0.15 cm/24 h in Table 2 is the large negative CPD of ~ -0.96 V. As seen in Table 1, the negative value of CPD is directly related to the O or OH in the outer atomic layer.

Table 3 shows the effect of temperature and time of immersion (in the H_2SO_4/dichromate solution) on the surface properties of the steel and endurance of the stainless steel-epoxy bond. The results of Table 3 are consistent with those of Table 2, showing that increasing dichromate concentration, the time of immersion or temperature change the surface properties and increases the bond endurance.

Durability from Morphology

It has recently been discovered for aluminum[4] and titanium[5] that microroughness (mechanical interlocking between adhesive and substrates) accounts for the enhanced durability of adhesive joints under hydrothermal stress. There is usually a poor correlation between

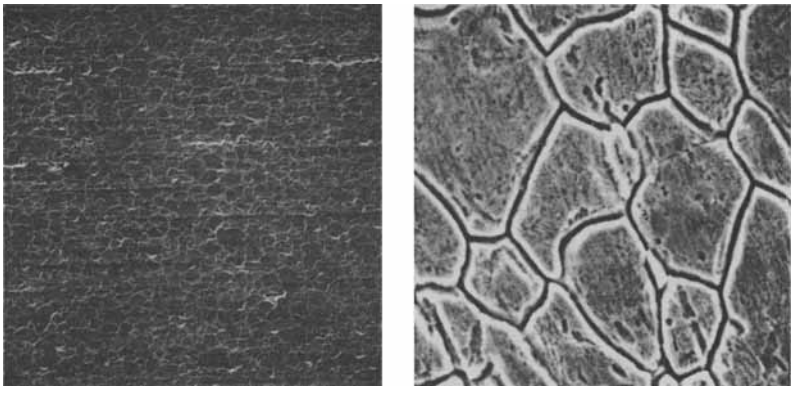

m. 10μ ⊔, 200x n. 1μ ⊔, 2000x

H_2SO_4/DICHROMATE
(PROCEDURE 12e)

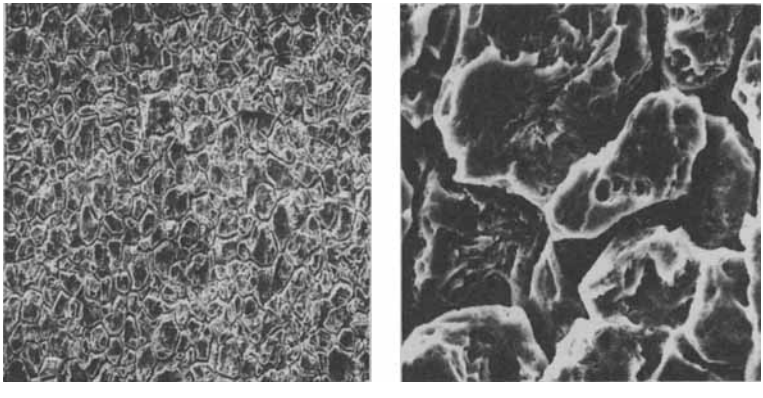

o. 10μ ⊔, 300x p. 1μ ⊔, 3000x

H_2SO_4/DICHROMATE ANODIZE
(PROCEDURE 7)

FIGURE 1 SEM photomicrographs for high endurance treatments.

endurance and macroscopic roughness as seen with the usual SEM. Microroughness that can be seen with scanning transmission electron microscopy (STEM[4,5]) seems to be of much greater importance. The

degree of interlocking will depend on the penetration and bonding in the pores, and this will, in turn, depend on the shape, dimensions, and surface chemistry of the porous structure.

The appearance of SEM pictures for the low endurance group is more smooth and shiny than for the high endurance group, which is a dull mat. SEM pictures of the low endurance group in Table 1, show little if any chemical attack.[1] Figure 1 shows SEM pictures representing the high endurance group; it is obvious that considerable chemical attack has occurred. In spite of the increased macroscopic roughness from procedure 7 as compared to procedure 12e (in Fig. 1), Table 1 indicates that the surface chemistry and microroughness of 12e produces as durable a joint as does procedure 7.

Although the SEM is unable to resolve the structure of the microroughness (mat layer) for procedure 12e, its nature is revealed by ellipsometry and water wettability measurements. For example, if a transparent (zero absorption index) oxide or hydroxide film is on a (microscopically) smooth metal, the ellipsometric value of the refractive index (n) will usually be close to the bulk value and $\kappa \sim 0$. Note that the ellipsometer is very sensitive to microscopic roughness (for roughness < wavelength of the light used) but rather insensitive to macroscopic roughness. This is because the ellipsometer is sensitive to the polarization state of the reflected light rather than the intensity. The ellipsometer ignores the light that is reflected away from the detector by macroscopic roughness and selectively monitors only the light reflected from facets with the proper angle of incidence. However, microscopic roughness changes the polarization states of the light that enters the detector.

If the oxide is porous and the substrate is smooth, the ellipsometer yields the film thickness and a refractive index less than the bulk value. The absorption index will remain approximately zero. If the oxide film is on a microscopically rough metal surface, the ellipsometer sees the roughness layer as a composite absorbing film with refractive index and absortion index between that of the metal and of the ambient. According to this analysis, procedures 5, 13a, 7, 12e, and 10h, in Table 1, that yield large values for κ, should have microscopic roughness.

If the microscopic roughness is in the form of interconnected channels, either as grooves or capillary tunnels, capillary action will drive the fluid through the channels and leave a spherical shaped cap in the center, as shown in the insert of Fig. 2. This type of wetting is observed for the processes with large κ and not for those with $\kappa \sim 0$.

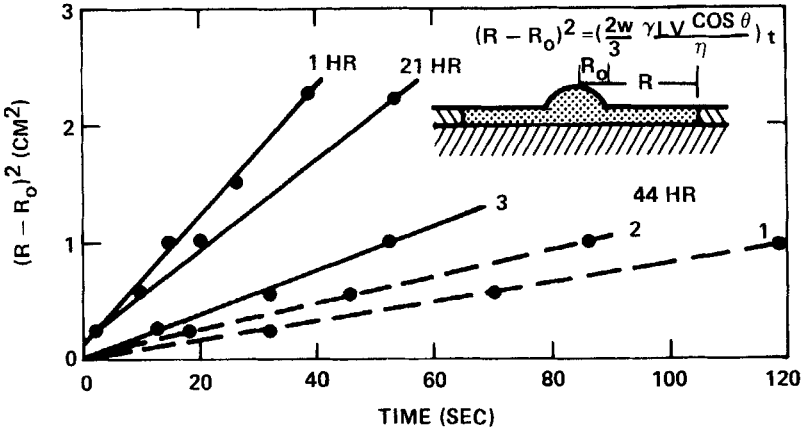

FIGURE 2 Expansion of a spreading drop on HNO_3-anodized stainless steel.

DISCUSSION OF ENDURANCE MECHANISMS

Durability from Chemistry

The dramatic drop in water contact angle for the durable group as compared to the nondurable group in Table 1, suggests that the nondurable surface treatments left organic contamination whereas the durable treatments did not. Two observations negate this idea; first, the APPH for carbon is not very different for the two groups and second, it was often found that surfaces with very low contact angles were not stable under hydrothermal stress (see Table 2). It is concluded that wettability is necessary but not sufficient for durability.

Figure 3 is a plot of hydrothermal stress endurance (solid points) and APPH(Cr) (open circles) *vs* the oxygen content of the outer surface of the oxide layer. The oxygen content $[O^{=} + OH^{-}]$ is given as the ratio of the APPH(O) to the maximum value ($\sim$9.6) from Table 1. The oxygen content varies from 0.25 to 0.5 for those films with no chromium in the outer layer (*i.e.*, Fe-oxide) and from 0.5 to 1.0 for those films with some Fe, but primarily Cr-oxide. Figure 3 shows that the hydrothermal-stress endurance increases dramatically with increasing

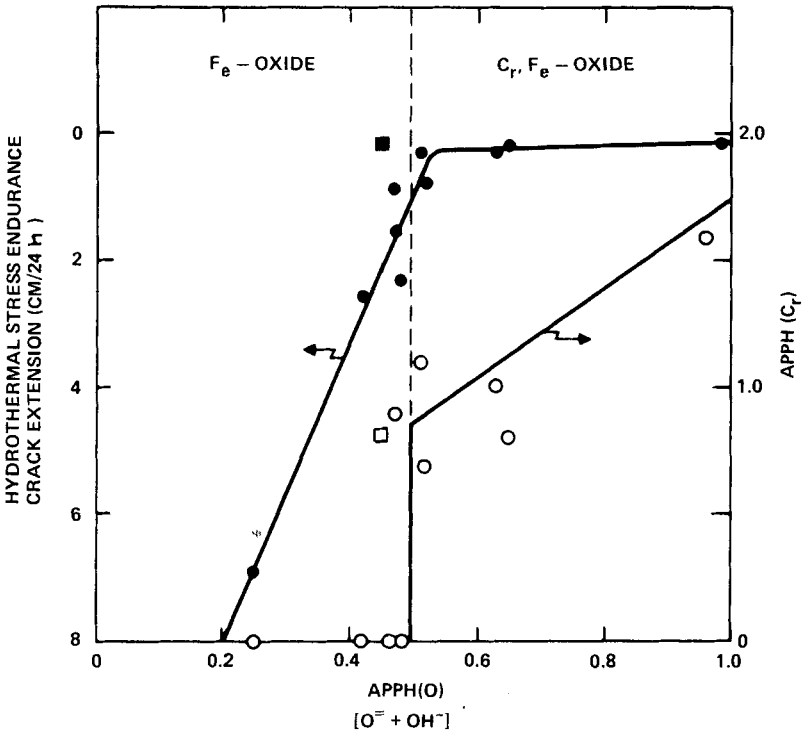

FIGURE 3 Endurance of stainless steel-adhesive bonds *vs* oxygen content in the outer atomic layer, after various surface treatments.

oxygen content, becoming excellent (crack extension ~ 0) for Cr, Fe-oxide.

To rationalize this result,[9] Figure 4 shows the schematic representation of the concentration of defects and adsorbed oxygen, on p-type semiconductor films, insulator films and n-type semiconductor films. In p-type semiconductor films all of the cations can act as electron donors so that the amount of oxygen adsorption is generally limited by the number of surface sites or the film thickness (number of cations). In the case of n-type semiconductors the electron donors are limited to the concentration of interstitial cations or anion vacancies (a very small number) so that oxygen adsorption is small. Insulating films

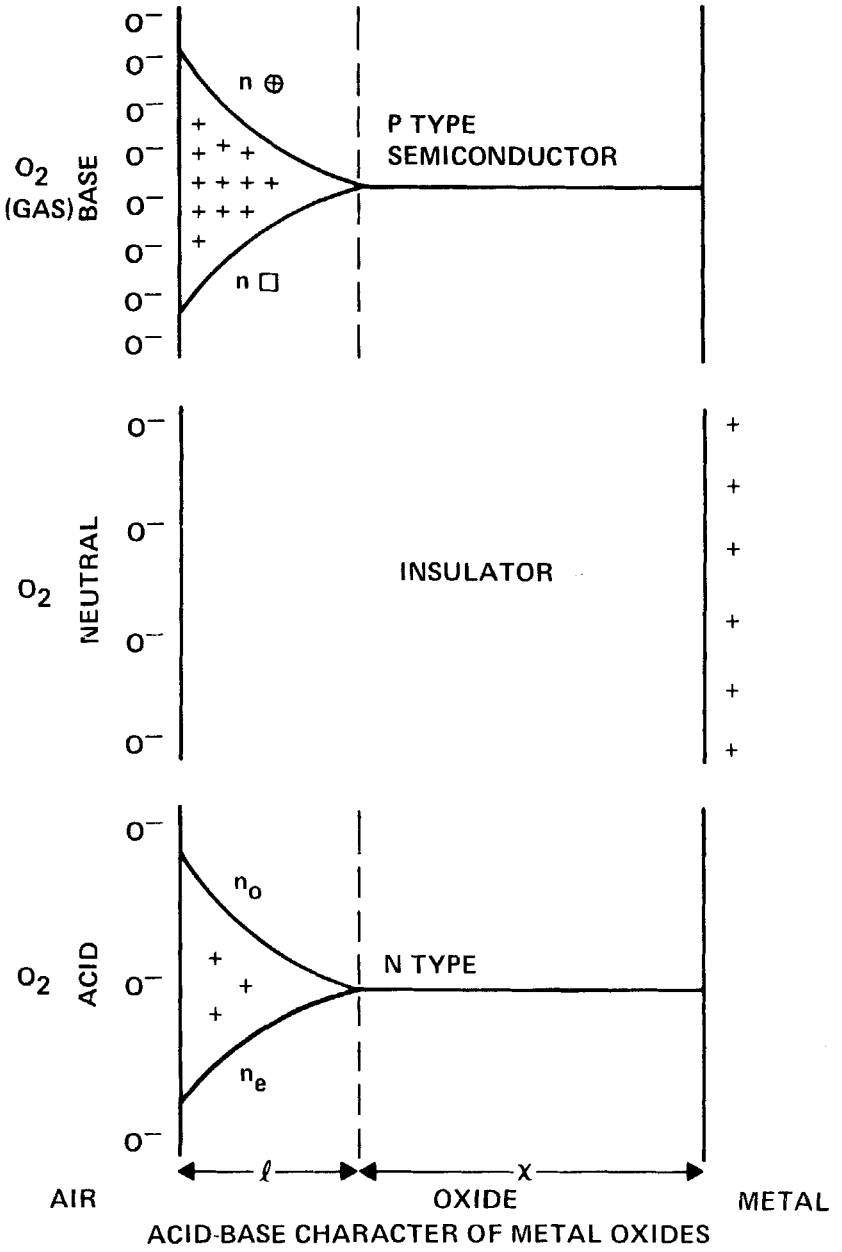

FIGURE 4 Schematic representative of semiconductor properties effect on oxygen adsorption.

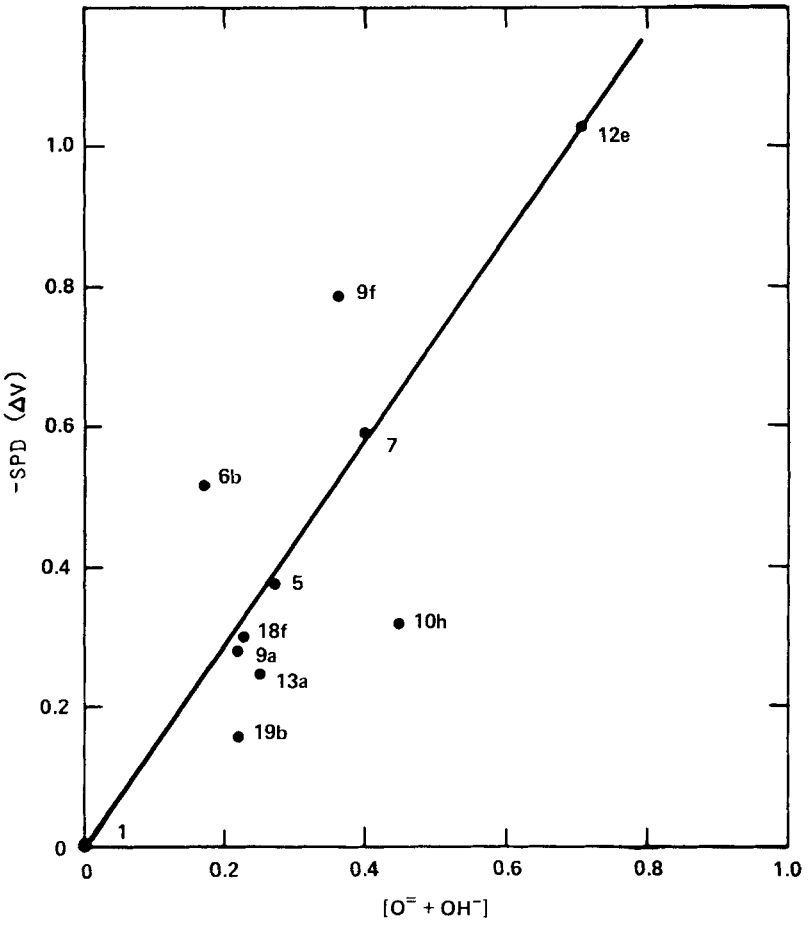

FIGURE 5 -SPD *vs* oxygen surface concentration after various surface treatments of steel. (The numbers relate to Table 1.)

adsorb oxygen, depending on the metal work function, the film thickness and dielectric properties.

If the film is very thin, such that the thickness d < l, the Helmholtz relation holds,[7]

$$\text{SPD} \sim \pm 4\Pi\mu\Gamma/D \tag{1}$$

where SPD is the change in CPD, μ is the effective dipole moment of the adsorbed molecules, Γ is the concentration of the adsorbate, and

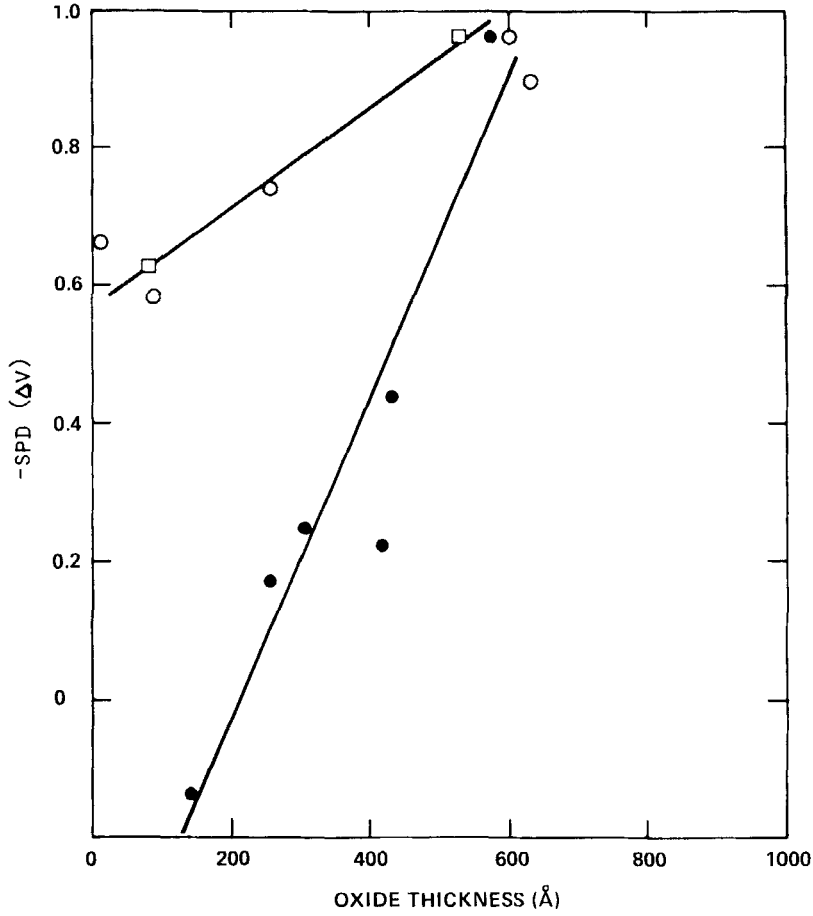

FIGURE 6 SPD *vs* film thickness for steel treated in H_2SO_4/dichromate as a function of dichromate concentration (●) and temperature (○). Average at 23°C and 80°C (□).

D is the dielectric constant of the film. SPD is positive if the dipole has the positive end pointing away from the surface and is negative for the negative end pointing away. Figure 5 shows that SPD becomes more negative with increasing oxygen surface concentration, as expected. The scatter of data in Figure 5 results for different values of D and μ, associated with the different surface treatments.

Figure 6 is a plot of SPD *vs* ellipsometric film thickness (from Tables 2 and 3) for the H_2SO_4/dichromate treatment at different dichromate

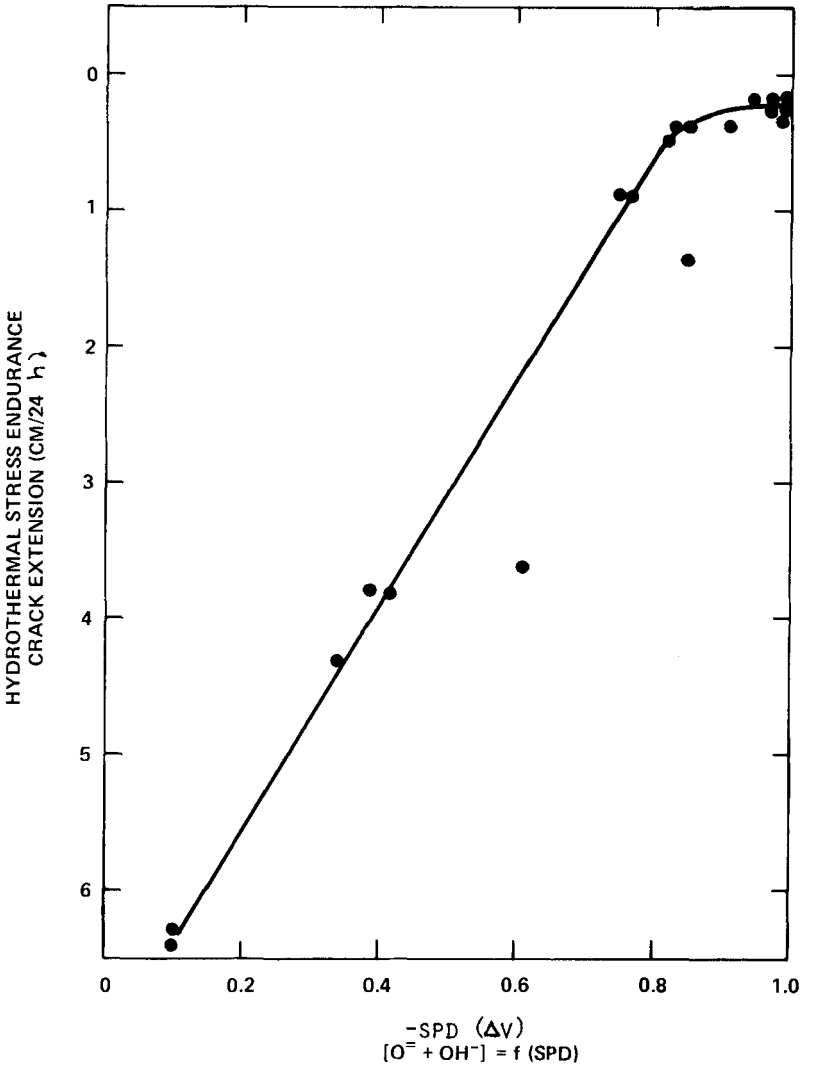

FIGURE 7 Hydrothermal stress endurance *vs* (SPD) for steel treated with H_2SO_4/dichromate.

concentrations (●) and different temperatures (○) (average values (□) at 23° and 80°C) from Table 3. Assuming that the surface concentration Γ depends on the number of cations in the film (p-type semiconductor),

and therefore on the film thickness, the relationships in Figure 6 are anticipated.

Figure 7 is a plot of hydrothermal stress endurance (decrease in crack extension) as a function of -(SPD) (*i.e.*, oxygen concentration) from Table 2 and 3. From Figure 3, very low crack extension begins at about 0.6 oxygen content. This corresponds to about −0.85 V in Figure 5. At −0.85 V in Figure 7 the endurance has maximized, consistent with Figure 3.

The following reactions are hypothesized.

Solid State-Surface Reactions in Etchant and Rinse

$$2Fe^{+2} + 2S + H_2O \overset{k_1}{\rightleftharpoons} 2Fe^{+3} + S\begin{matrix}O^{=}\\ \diagup\ \diagdown\\ S\end{matrix} + H_2\uparrow \tag{2}$$

$$1/3Cr^{+3} + S + H_2O \overset{k_2}{\rightleftharpoons} 1/3Cr^{+6} + \underset{\displaystyle OH^{-}}{\underset{|}{S}} + 1/2H_2\uparrow \tag{3}$$

Reactions in Stress Environment

$$2Fe^{+2} + 2S\text{-}A + H_2O \overset{k_{14}}{\rightleftharpoons} 2Fe^{+3} + S\begin{matrix}O=\\ \diagup\ \diagdown\\ S\end{matrix} + H_2\uparrow + A(H_2O) \tag{4}$$

$$\begin{matrix}O^{=}\\ \diagup\ \diagdown\\ (S\quad S)\end{matrix}A + H_2O \overset{k_{34}}{\rightleftharpoons} \underset{|}{S}\begin{matrix}O^{-}\text{-}H\ldots O^{-}\text{-}H\\ \qquad\quad |\\ \qquad\quad S\end{matrix} + A(H_2O) \tag{5}$$

Equations (2) and (3) are for oxidation of oxide-film cations by water to form chemisorbed anions. It has been demonstrated by[8,9] ESCA that Fe-oxides chemisorb oxygen (Eq. (2)), whereas the presence of chromium in the oxide allows chemisorption of OH^- (reaction 3). The symbol S represents surface sites that have not chemisorbed $O^=$ or OH^-. The symbol $\begin{matrix}O^{=}\\ \diagup\ \diagdown\\ S\quad S\end{matrix}$ represents oxygen chemisorbed on two sites (S_2-$O^=$) and S-OH^- is OH^- chemisorbed on a single site, probably as

$$\begin{matrix}O^{-}\text{-}H..O^{-}\text{-}H..O^{-}\text{-}H.\\ |\qquad\ |\qquad\ |\\ S\qquad S\qquad S\end{matrix}$$

Reactions 2 and 3 occur in the acid solution and water rinse. Since hydrogen is removed from the reaction zone, given sufficient time these reactions go to completion, such that the concentration of $S_2\text{-}O^{=}$ and $S\text{-}OH^{-}$ are limited by the time of reaction or the number of electron donors in the film. As indicated in Figure 6, it follows that the oxygen surface concentration is directly related to the oxide film thickness and form, since

$$(S_2\text{-}O^{=}) = (1/2)(Fe^{+2}).d \tag{6}$$

$$(S\text{-}OH^{-}) = 3(Cr^{+3}).d, \tag{7}$$

where $(S_2\text{-}O^{=})$ and $(S\text{-}OH^{-})$ refer to the concentration of chemisorbed ions per cm^2, and (Fe^{+2}) and (Cr^{+3}) refer to the concentration of cations in the oxide film.

After removing the steel from the rinse water, drying, and adhesive bonding, reactions 4 and 5 can begin. Reaction 4 is the splitting of bonds between surface sites S and adhesive (*i.e.*, S-A) to form $\overset{O^{=}}{\underset{S}{/}\quad\backslash\underset{S}{}}$ and the reaction product between water and the adhesive $A(H_2O)$. Reaction 5 is the splitting of bonds between surface sites $\overset{O^{=}}{\underset{S}{/}\quad\backslash\underset{S}{}}$ and adhesive $(\overset{O^{=}}{\underset{S}{/}\quad\backslash\underset{S}{}})A$, to form $\overset{O^{-}\text{-}H\ldots O^{-}\text{-}H}{\underset{S}{|}\qquad\quad\underset{S}{|}}$ and $A(H_2O)$. If the crack extension is controlled by reactions 4 and 5, the total extension rate can be expressed

$$da/dt = k_{1A}(S\text{-}A)^2(H_2O) + k_{3A}\left(\overset{O^{=}}{/\quad\backslash}\right)A.(H_2O) \tag{8}$$

where the concentration of unreacted sites (S-A) is,

$$(S\text{-}A) = N - (S\text{-}OH^{-})A - 2(S_2\text{-}O^{=})A \tag{9}$$

and N is the total number of sites per cm^2. Equation (8) predicts the crack extension rate to follow two limiting forms, as observed for the Fe-oxide and Cr, Fe-oxide regions in Figure 3. At the left, the Fe-oxide region, $(S\text{-}OH^{-})$ and $(S_2\text{-}O^{=})$ are low, and from Eq. (9) $(S\text{-}A) \rightarrow N$, so that da/dt is large. As $(S_2\text{-}O^{=})$ increases according to reaction 2, for Fe-oxide, there is a linear decrease in da/dt until $2(S_2\text{-}O^{=}) \sim N$, at which point $(S\text{-}A) \rightarrow 0$, and reaction 4 ceases. For the Cr,Fe-oxide region, reaction 5 predominates, but decreases linearly as $(S\text{-}OH^{-}) \rightarrow N$.

A particularly interesting aspect of this model is the prediction that the maximum oxygen concentration on Cr,Fe-oxide will be just double that on Fe-oxide, since it takes two sites for O^- adsorption and one site for OH^-. The experimental confirmation of this model is observed by $[O^- + OH^-] = 0.5$ at the point the oxide becomes Cr,Fe-oxide in Figure 3, indicating that reaction 2 is essentially complete, before reaction 3 begins.

This model explains why some surface treatments yield durable adhesive joints for stainless steel under hydrothermal stress and others do not. After removal from the acid-etch and rinse water, the surface sites are occupied by $O^=$ or OH^- (*i.e.*, electron-rich basic sites), which react strongly with acid-type functional groups of the epoxy adhesive. Fracture of the bond under dry conditions is cohesive in the adhesive and, during hydrothermal exposure, there is no thermodynamic driving force for degradation if all sites are occupied by OH^-. If the sites are occupied by $O^=$, a very slow reaction can occur (reaction 5); if the sites are empty, rapid degradation can occur *via* reaction 4.

Hydrothermal-stress endurance results from a surface treatment that provides a p-type oxide film. This film should be thick enough to provide enough electrons to saturate the surface with OH^-.

To evaluate the effect of temperature and mechanical stress, consider the absolute reaction rate theory for the rate constants k_{1A} and k_{3A},

$$k_{1A,3A} = (\kappa kT/h)e^{\frac{\Delta S^{\ddagger}}{k}} e^{\frac{-\Delta H^{\ddagger}}{kT}}. \tag{10}$$

In Eq. (10) κ is the transmission coefficient, k is the Boltzmann factor, h is Planck's constant, T is the absolute temperature, $\Delta S^{\ddagger}$ is the activation entropy, and $\Delta H^{\ddagger}$ is the activation enthalpy. Since $\Delta H^{\ddagger}$ is positive, increasing temperature will increase $k_{1A,3A}$ and therefore da/dt.

The stress intensity at the crack tip can act to decrease the activation energy for crack growth. The stress intensity at the crack tip is just equal to the fracture toughness G_I, so that $\Delta H^{\ddagger}$ can be replaced by

$$\Delta H^{\ddagger}_{\text{eff}} = (\Delta H^{\ddagger} - \alpha G_I). \tag{11}$$

In Eq. (11), α is a proportionality constant. Unless G_I acts to decrease (H_2O) at the crack tip, G_I will always act to increase the degradation rate exponentially, by lowering the effective activation enthalpy.

Durability from Morphology

The capillary effect on the sessile drop has been observed[10] before and analyzed to yield the following equation:

$$(R - R_0)^2 = [(2/3\ \gamma_{LV}\ w \cos \theta/\eta] \times t. \quad (12)$$

In Eq. (12), R is the distance the fluid has traveled at time t, R_0 is the radius of the drop, γ_{LV} is the liquid surface tension, θ is the contact angle in the capillaries, η is the fluid viscosity, and w is the channel width of the capillaries.

As an example of microroughness, Figure 2 gives $(R - R_0)^2$ *vs* t for procedure 10h (HNO_3 – anodize). The steepest line was measured 1 h after anodizing; the next 21 h after and the lower lines labeled 1, 2, and 3 were measured 44 h after anodizing. Lines 1, 2, and 3 are for measurements reported immediately after each other and with drying between the measurements. All of the curves follow the theoretical linear relationship between $(R - R_0)^2$ and t.

The decreasing slope with laboratory aging is due to contamination from the laboratory air, which results in an increasing capillary contact angle θ and thus a decrease in cos θ. The increasing slope of curves 1, 2 and 3 is due to removal of part of the contamination by the water used in the measurements.

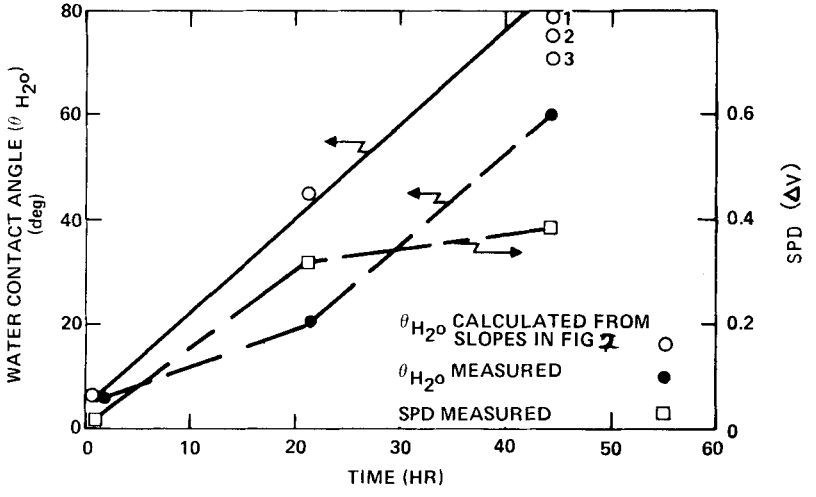

FIGURE 8 Water contact angle and SPD *vs* laboratory aging time.

Figure 8 gives the contact angle (open circles) calculated from the slopes of the curves in Figure 2, assuming that the initial value of the capillary contact angle was the same as that of the initial central drop ($\sim 5^{\circ}$). The measured contact angles of the central cap (solid points) follow the same trend as within the capillaries but are somewhat lower. The positive increase in SPD (curve □, Fig. 8) corresponds to the usual increase due to organic contamination, with positive end (hydrocarbon tail) pointing away from the surface.

Figures 2 and 8 leave little doubt as to the capillary nature of the microroughness associated with the HNO_3-anodize and the other surface treatments with large absorption index κ. It also explains why HNO_3-anodize treatment has very high hydrothermal-stress endurance even though the oxygen surface concentration is low. In Figure 3 the symbol ■ represents the crack extension and □, the APPH(Cr) for HNO_3-anodize treatment. It is believed that mechanical interlocking of the adhesive in the microrough (capillary) layer has increased the endurance beyond that predicted from surface chemistry alone (upper curve in Fig. 3). In contrast, procedure 9f (HNO_3-dichromate) and 13b (H_2SO_4-HNO_3-dichromate) have microscopically smooth substrates (as noted by the ellipsometric absorption index of zero) and wetting without the "capped drop". However, the high concentration of adsorbed oxygen indicates reaction completion with water and yields strong bonding and chemical stability without microroughness.

Calculation of a typical capillary channel width w, from the slopes of $(R\text{-}R_0)^2$ *vs* t and Eq. (12) yields $w \sim 300$Å, which is of the same order as the ellipsometric thickness of the microroughness film (see Table 1). Ellipsometric measurement of the thickness of the roughness film filled with water reveals that the added water has an effective thickness of approximately 250Å in the middle of the ring (R/2) and about 100Å at the ring edge (R). These results are of the same order as the dimension of the capillary channels (d = 300Å).

The question of how this capillary layer is formed can best be answered with Olefjords[4,9] mechanism of surface transformation during the passivation of stainless steel. Strongly oxidizing solutions (acids with dichromates) and anodic treatments can selectively dissolve iron from the Fe, Cr, Ni, Mo alloy matrix. Auger spectroscopy and XPS have revealed (Refs. 9, 10 and this work) the chemical nature of the transformed surface. The outer layer is primarily chromium oxide, but an intermetallic layer highly enriched in Cr, Ni, and Mo is formed just beneath the oxide. There must be a reprecipitation of this intermetallic

layer following dissolution of the alloy. Although the chemistry of this precipitated layer is revealed by Auger spectroscopy and XPS, the physical capillary structure is revealed by ellipsometry and the water wetting "capped drop" phenomenon. The reprecipitated intermetallic layer must form a dendritic open structure that acts as extremely fine, connected capillaries or channels. This microroughness greatly increases the surface area of adhesive bonding as well as provides pores for mechanical interlocking.

CONCLUSIONS

The hydrothermal-stress endurance of stainless steel bonded with epoxy depends on the surface chemistry and surface morphology (roughness). If the surface treatment leaves the surface with all sites covered with chemisorbed base OH^-, which bonds strongly to acid functional groups in the epoxy, there is no thermodynamic driving force for further reaction with water. These surface treatments are stable under hydrothermal stress and are very durable. Those surface treatments that leave the surface with no adsorbed OH^- are thermodynamically unstable and will react with water after bonding. These treatments yield nondurable adhesive joints.

The formation of microroughness during the surface treatment can relax the dependence on proper surface chemistry and, through mechanical interlocking, greatly enhance the durability of joints. It is hypothesized that in strongly oxidizing surface treatments, the outer layers of the steel alloy dissolve and that a Cr, Ni, Mo intermetallic layer reprecipitates in the form of a chromium-oxide-coated, dentritic, capillary structure. This layer appears to the ellipsometer as a film a few hundred angstroms thick with the absorption properties of the metal-void-oxide mixture even though the chromium oxide layer on the dentrites is only of the order of 20–50Å as for the normal passive layers. If the film is a capillary film of Cr metal covered with a very thin passive oxide, the question is still open as to why the value of -SPD (surface oxygen concentration) is proportional to the film thickness. However, the mechanism of electron transfer from the thin chromium oxide and the relationship between the concentration of adsorbed oxygen and film thickness to chemisorb OH^- or $O^=$ remains the same, if it is assumed that a direct relationship exists between the

thickness of the passive chromium oxide film on dentrites and the effective thickness of the dentritic layer.

References

1. R. Haak and T. Smith, *Int. J. Adhesion and Adhesives*, p. 15, Jan. 1983.
2. T. Smith, "Specialized Cleaning, Finishing and Coating Processes," Proceedings of a Conference held 5–6 Feb. 1980, Los Angeles, CA, Materials/Metalworking Technology Series, American Society for Metals, p. 49.
3. T. Smith, *J. Appl. Phys.* **46**, 1553 (1975).
4. J. D. Venables, *et al.*, 10th National SAMPE Technical Conference, **10**, 362 and **12**, 981 (1978).
5. B. M. Ditchek, *et al.*, 25th National SAMPE Symposium, **25**, 131 (May 1980).
6. K. Hauffe, *Oxidation of Metals* (Plenum Press, New York, 1965), p. 99.
7. R. V. Culver and F. C. Tompkins, *Advan. Catalysis* **11**, 74 (1959).
8. I. Olefjord, private communication.
9. I. Olefjord and B. Elpstrom, Corrosion/81, The International Corrosion Forum Sponsored by the National Association of Corrosion Engineers/April 6–10, 1981/ Sheraton Center, Toronto, Ontario, Canada.
10. G. D. Cheever, "Wetting of Phosphate Interfaces by Polymer Liquids," in *Interface Conversion for Polymer Coatings*, P. Weiss and G. D. Cheever, Eds. (American Elsevier Publishing Co., New York, 1968), p. 150.